Conformational Dynamics of Charge-Transfer States in Donor−Bridge−Acceptor Systems

Xavier Y. Lauteslager,[a] Ivo H. M. van Stokkum,[b] H. John van Ramesdonk,[a] Dick Bebelaar,[c] Jan Fraanje,[d] Kees Goubitz,[d] Henk Schenk,[d] Albert M. Brouwer,*[a] and Jan W. Verhoeven*[a]

Keywords: Charge-transfer / Conformation analysis / Donor−acceptor systems / Electron transfer / Fluorescence

Donor–acceptor compounds containing a phenylenediamine electron donor and a naphthalene, a cyanobenzene, or a cyanonaphthalene acceptor were studied. The two chromophores are connected by three different bridging units, consisting of CH_2 groups linked to a semiflexible piperidine or piperazine ring or to a rigid 2,5-diazabicyclo[2.2.1]heptane group. All donor–acceptor compounds show photoinduced charge separation, resulting in the formation of a compact charge-transfer (CCT) state in nonpolar solvents. The conformational change needed to arrive at this species is impossible in a nonpolar polymer matrix and also in methylcyclohexane at low temperature. In the cases of the piperidine- and piperazine-bridged donor–acceptor compounds, evidence for the involvement of an extended charge-transfer (ECT) species as a precursor of the CCT species was obtained from time-resolved fluorescence measurements. In contrast to harpooning systems studied previously, the energy differences between the species in the present case are so small that their interconversions are reversible within the excited state lifetimes.

Introduction

Electron transfer between an electron donor D and an electron acceptor A can create charge-transfer states (D^+A^-) with charge separation distances as large as ca. 1 nm.[1] Because of the electrostatic attraction between D^+ and A^-, structural changes that bring the charged groups closer together can occur subsequently. This "harpooning" process was first described for the interaction between alkali metal and halide atoms,[2] but has also been found to occur in molecular systems in solution.[3−7] The prototype compound **1** illustrates the interconversion between a spatially extended charge-transfer excited state (ECT) and a more compact CT state labeled CCT (Scheme 1). We have previously shown that the photoinduced harpooning process is effectively suppressed when the piperidine bridge (e.g., compounds **1** and **2**, Scheme 2) is replaced by a piperazine bridge (e.g., compound **3**).[8]

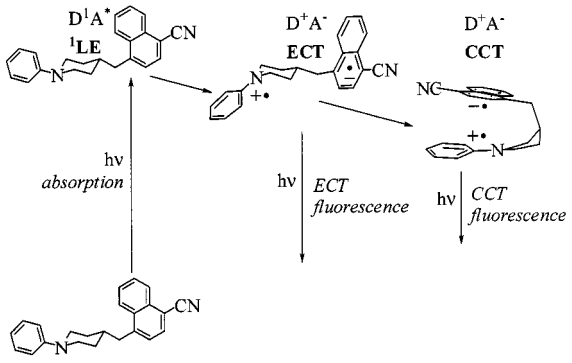

Scheme 1. The harpooning process, illustrated for compound **1**

Although the conformational flexibility of the piperazine ring is similar to that of the piperidine ring, the charge distribution in the initially formed charge-transfer state is very different for the two systems: In donor−acceptor compounds **1** and **2** the positive charge resides on the (methoxy)-aniline group, yielding an ECT species with a dipole moment of ca. 30 D.[9,10] Piperazine-bridged systems such as **3**, on the other hand, can be regarded as (D_2-D_1-A) triads, the trialkyl-substituted nitrogen atom acting as an electron donor group D_1.[11] Trapping of the positive charge on D_1 to yield a $D_2-D_1^+-A^-$ species prevents the formation of an extended CT (ECT) state ($D_2^+-D_1-A^-$) and thereby also precludes the electrostatically driven folding from ECT to CCT. In radical cations of piperazines

[a] Institute of Molecular Chemistry, University of Amsterdam, Laboratory of Organic Chemistry,
Nieuwe Achtergracht 129, 1018 WS Amsterdam, The Netherlands
Fax: (internat.) + 31-20/525-5670
E-mail: fred@org.chem.uva.nl
[b] Faculty of Sciences, Vrije Universiteit Amsterdam,
De Boelelaan 1081, 1081 HV Amsterdam, The Netherlands
[c] Institute of Molecular Chemistry, University of Amsterdam, Laboratory of Physical Chemistry,
Nieuwe Achtergracht 129, 1018 WS Amsterdam, The Netherlands
[d] Institute of Molecular Chemistry, University of Amsterdam, Laboratory of Crystallography,
Nieuwe Achtergracht 166, 1018 WV Amsterdam, The Netherlands
Supporting information for this article is available on the WWW under http://www.wiley-vch.de/home/eurjoc or from the author.

  1434−193X/01/0816−3105 $ 17.50+.50/0

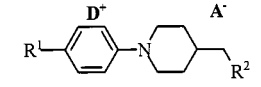

1 R^1 = H, R^2 = 1-(4-cyanonaphthyl)
2 R^1 = MeO, R^2 = 1-(4-cyanonaphthyl)

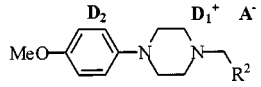

3 R^2 = 1-(4-cyanonaphthyl)

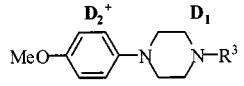

4 R^3 = alkyl or aryl

Scheme 2. Compounds studied in previous work

(D_2-D_1), the positive charge tends to be delocalized over both nitrogen atoms,[12] but stabilizing methoxyphenyl substituents in the free radical cations suffice to localize the charge on the neighboring amino group, giving rise to a $D_2^+-D_1$ charge distribution (as in compound **4** in Scheme 2).[13−15]

The localization of the positive charge on D_1 ($D_2-D_1^+-A^-$) in piperazine **3** is a result of the electrostatic interaction with the nearby A^-. If the oxidation potential of D_2 were lower, it should be possible to reach the fully extended CT state ($D_2^+-D_1-A^-$) and so restore the harpooning mechanism. In this study we decided to incorporate a phenylenediamine unit as the electron donor. This is easier to oxidize than a methoxyaniline, by roughly 0.4 eV, and can form stable radical cations.[16,17] We compare the piperazine systems **5a**−**5d** with corresponding compounds **6a**, **6b**, and **6d**, all with a piperidine bridge, and compounds **7a**−**7d**, all with a conformationally rigid (1*S*,4*S*)-2,5-diaza[2.2.1]bicycloheptane bridge (see Scheme 3). Although ring inversion is precluded in compounds **7a**−**7d**, nitrogen inversions and rotation around the C−C bonds of the methylene group are still possible.

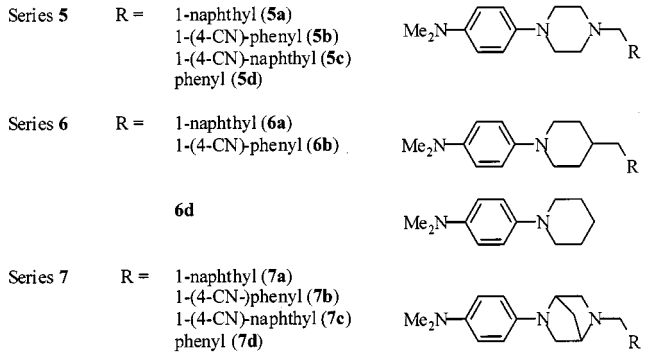

Scheme 3. Compounds under study

Because one of the amino groups of the phenylenediamine unit is part of the bridge, the structure of the bridge can have a significant effect on the photophysical and electrochemical properties of the phenylenediamine unit. For this reason, the choice of model compounds used to determine the photophysical properties of the donor unit in the absence of the acceptor required special attention. Electron acceptor groups employed were the 1-naphthyl group (compounds **a**; E_{red} = −2.58 V vs. SCE[18]), the 4-cyanophenyl group (compounds **b**; E_{red} = −2.2 V[18]), and the 4-cyano-1-naphthyl group (compounds **c**; E_{red} = −1.91 V[5]).

Results and Discussion

Synthesis

N-(4-Dimethylaminophenyl)piperazine was synthesized as shown in Scheme 4. *N*-Benzylpiperazine was coupled with 1-fluoro-4-nitrobenzene,[19] and the nitro group of the obtained compound was reduced with sodium borohydride.[20] Methylation of the obtained *N*-(4-aminophenyl)-*N*′-benzylpiperazine with (para)formaldehyde and sodium borohydride was performed using the method of Giumanini et al.[21]

The compound **5d** thus obtained was able to serve nicely as a model donor compound, incorporating the phenylenediamine donor, but lacking an electron-accepting group. Debenzylation of this compound yielded the desired piperazine, which could be coupled to different bromomethyl-substituted aromatic compounds. As (1*S*,4*S*)-*N*-benzyl-2,5-diazabicyclo[2.2.1]heptane dihydrobromide was commercially available, we were able to follow the same route as just described for *N*-benzylpiperazine. Compound **7d** in this route could be used as a reference donor compound.

The synthesis of piperidine-bridged donor−acceptor systems (Scheme 5)[22] starts with the preparation of the appropriate piperidone by means of a cyclization reaction between dimethylamino-*p*-phenylenediamine and 1,5-dichloro-3-pentanone. The piperidone can be coupled by Wadsworth−Emmons condensation to various phosphonates to introduce the aromatic chromophores. Reduction of the exocyclic double bond finally produces the desired systems. A model donor compound (**6d**) was available in our laboratory.[14]

Model Donor Compounds

UV-Absorption Spectra of the Model Donor Compounds

Compounds **5d**, **6d**, **7d**, and *N*,*N*,*N*′,*N*′-tetramethyl-*p*-phenylenediamine (TMPD) served as models for the *p*-phenylenediamine unit. The maxima and molar absorption coefficients of the ^1L_a and ^1L_b bands observed for all these compounds are given in Table 1.

The positions of the ^1L_b bands of **5d** and **6d** are identical, but those of TMPD and **7d** are bathochromically shifted. The largest difference (1400 cm^{-1}) is observed between **5d** and **7d** (Figure 1). As we show below, the oxidation potentials of **7d** and **5d** differ significantly as well.

Fluorescence of the Model Donor Compounds

The fluorescence spectra of the model donor compounds **5d**−**7d** were recorded in cyclohexane and diethyl ether. All

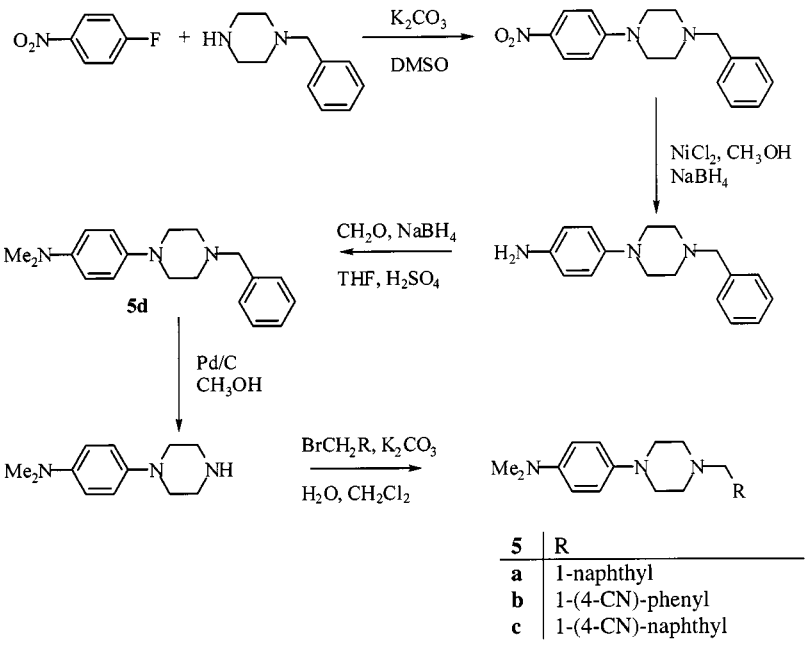

Scheme 4. Synthesis of the piperazine-bridged donor−acceptor systems

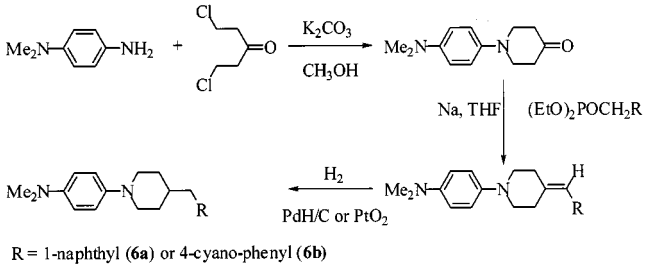

Scheme 5. Synthesis of the piperidine-bridged donor−acceptor systems

Table 1. Absorption maxima [nm] and molar absorption coefficients [M^{-1} cm^{-1}] (in parentheses) of the ^1L_a and ^1L_b bands of the phenylenediamine model donor compounds in cyclohexane

Compound	^1L_a transition	^1L_b transition
TMPD	264 (15970)	327 (2410)
5d	264 (18040)	319 (2260)
6d	265 (16700)	319 (2360)
7d	267 (18610)	334 (2570)

compounds show characteristic fluorescence around 390 nm upon excitation at 308 nm. A slight solvent dependency in the position of this band is observed. The quantum yields and decay times of fluorescence of the four compounds in cyclohexane and diethyl ether are listed in Table 2.

TMPD and compound **7d** show similar radiative and nonradiative rate constants in the two solvents. Compounds **5d** and **6d** also show almost identical behavior. For the latter two, this is not surprising as the phenylenediamine chro-

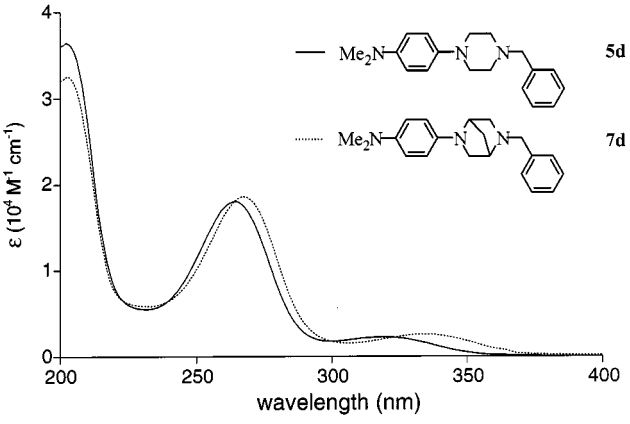

Figure 1. UV-absorption spectra of **5d** and **7d** in cyclohexane

Table 2. Quantum yields, decay times [ns], and rate constants [10^6 s^{-1}] of fluorescence (k_f), and nonradiative decay (k_d) of the reference donor compounds in cyclohexane and diethyl ether

	Cyclohexane				Diethyl ether			
Compound	Φ_f[a]	τ[b]	k_f	k_d	Φ_f	τ	k_f	k_d
TMPD	0.18	4.3	42	191	0.20	5.1	39	157
5d	0.12	3.4	35	259	0.11	3.9	28	228
6d	0.11	3.5	31	254	0.11	4.5	24	198
7d	0.24	5.3	45	143	0.24	6.0	40	127

[a] Quinine bisulfate in 1 N H_2SO_4 (Φ = 0.546) or anthracene in cyclohexane (Φ = 0.18)[46] used as standards. − [b] Determined by means of time-correlated single photon counting; decays were measured at three different wavelengths and could be fitted very well with a single exponential function.

mophores are expected to be geometrically very similar. However, this also implies that the trialkyl-substituted nitrogen atom in **5d** does not influence the photophysical properties of the phenylenediamine part. The similar values for TMPD and **7d** also point to comparable phenylenediamine chromophore conformations. The crystal structure of compound **7c** has been resolved and is presented below, where we again address this issue.

Oxidation Potentials of the Model Donor Compounds

With three of the compounds, oxidation potentials were measured by cyclic voltammetry. Ferrocene was used as an internal standard.[23,24] The oxidation potentials are referenced to SCE, taking a value of 0.45 V versus SCE for ferrocene in acetonitrile.[25] TMPD shows two reversible oxidation waves at 0.17 and 0.76 V versus SCE in acetonitrile. Compounds **5d** and **7d**, however, each show only one reversible oxidation wave, at 0.26 and at 0.14 V versus SCE, respectively. The presence of the saturated trialkyl-substituted nitrogen atom probably causes the irreversibility of the second oxidation step, since − for example − this step is reversible in compound **6b**, showing up at 0.75 V versus SCE. The oxidation potential of **6d** was not measured, but might be expected to be close to that of **6b** (0.22 V versus SCE). The cyclic voltammograms, showing the first oxidation waves of three model donor compounds, are displayed in Figure 2. The oxidation potential(s), including those of two donor−acceptor systems, are listed in Table 3.

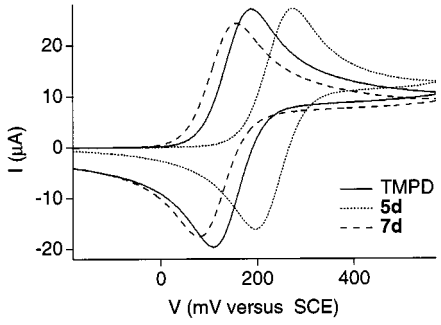

Figure 2. Cyclic voltammograms of TMPD, **5d**, and **7d** (circa 2 mM solutions in acetonitrile, 0.1 M tetrabutylammonium hexafluorophosphate as electrolyte)

Table 3. Halfwave oxidation potentials in acetonitrile [V] (versus SCE) of three model donor compounds and two donor−acceptor compounds

Compound	$E_{1/2}$ (ox1)	$E_{1/2}$ (ox2)
TMPD	0.17	0.76
5d	0.26	[a]
7d	0.14	[a]
5b	0.27	[a]
6b	0.22	0.75

[a] Irreversible.

The largest difference in oxidation potentials is found between **5d** and **7d**. This difference of circa 120 mV is surprisingly large, as the tetraalkylphenylenediamine units appear very similar. In the next section we show that small but significant geometrical differences are responsible for these observations.

Quantum Chemical Calculations of the Ionization Potentials and Excitation Energies

The simplest computational approach to address the question of why the oxidation potentials of **5d** and **7d** differ so much is to calculate the difference between the relaxed (adiabatic) ionization potentials of the two molecules [Equation (1)].

$$\mathbf{5d} + \mathbf{7d}^{+\bullet} \rightarrow \mathbf{5d}^{+\bullet} + \mathbf{7d} \quad (1)$$

If differences are caused by purely geometrical effects, the second amino group in the ring probably does not play a role. We therefore took *N*-phenylpiperidine and *N*-phenyl-2-azabicyclo[2.2.1]heptane as models for **5d** and **7d**, respectively. In principle, the latter compound can exist in two conformations, because the amino group is nonplanar. Only the most stable one (*endo*) will be considered. To perform the comparison represented in Equation (1), all calculations have to be done at the same level of theory. Following previous favorable experiences,[26,27] we chose to use the B3LYP hybrid Hartree−Fock/Density Functional method[28] with the 6-31G* basis set[29] to determine the vertical and relaxed ionization potentials (see Figure 3). The obtained results are given in Table 4.

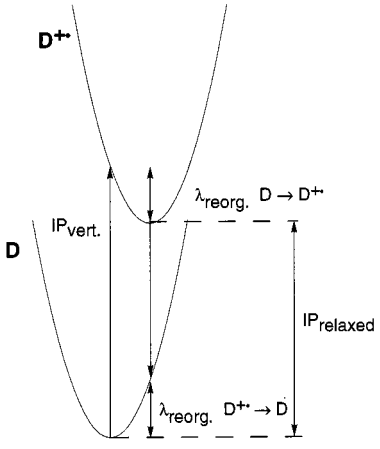

Figure 3. Schematic potential energy curves of the neutral and cation state, showing the reorganization energies and vertical and relaxed ionization potentials

Table 4. B3LYP/6-31G*-calculated ionization potentials and lowest excitation energies (eV) and oscillator strengths for *N*-phenylpiperidine and *N*-phenyl-2-azabicyclo[2.2.1]heptane

Compound	$IP_{vertical}$	$IP_{relaxed}$	E_{exc}	f
N-phenylpiperidine	6.70	6.33	4.68	0.0035
N-phenyl-2-azabicyclo[2.2.1]heptane	6.36	6.20	4.58	0.029

In *N*-phenylpiperidine, steric interactions between the phenyl ring and the α-CH_2 groups of the piperidine ring produce a significant twist angle between the rings and pyramidalization of the nitrogen atom (sum of the C−N−C bond angles ΣN = 334°, twist angle ω = 34°). In *N*-phenyl-2-azabicyclo[2.2.1]heptane, the steric interaction is smaller and conjugation between the lone pair and the benzene ring is more favored, as indicated by the smaller degrees of pyramidalization (ΣN = 353°) and twist (ω = 6°). In the radical cations, the nitrogen atoms are in a planar trigonal environment (ΣN = 360°), but in the case of *N*-phenylpiperidine there is still a twist angle of 17°, while in *N*-phenyl-2-azabicyclo[2.2.1]heptane this is only 4°. The computed difference between the relaxed ionization potentials of *N*-phenylpiperidine and *N*-phenyl-2-azabicyclo[2.2.1]heptane is 0.13 eV, which agrees remarkably well with the experimental difference in oxidation potentials between **5d** and **7d** of 0.12 V!

The less favorable conjugation in the piperidine system (and presumably also in the piperazine system) is also likely to be the reason for the different photophysical properties noted in the previous sections. Indeed, time-dependent DFT calculations[30] confirm that the lowest excitation energy is lower for the more conjugated *N*-phenyl-2-azabicyclo[2.2.1]heptane than for *N*-phenylpiperidine (Table 4).

Donor-Acceptor Systems

Crystal Structure of 7c and Structure of 7a in Solution

With compound **7c**, it was possible to obtain a crystal suitable for single-crystal X-ray analysis (Exp. Sect.). Crystals of **5c** were obtained as well, but the structure could not be resolved satisfactorily ($R \approx 0.22$) by X-ray analysis. From the analysis it was nevertheless clear that both the donor and the acceptor chromophores are in an equatorial position, as has been observed before for an analogous compound.[9] A presentation of the crystal structure of **7c**, with the numbering of the non-hydrogen atoms, is given in Figure 4.

Interestingly, both chromophores are in *endo* positions. Recently, low-temperature ^{13}C NMR measurements and molecular-mechanics calculations on 2-methyl-2-azabicyclo[2.2.1]heptane have been reported.[31] Experimentally, the *endo* isomer was also found to be about 1.2 kJ mol^{-1} more stable than the *exo* isomer in this compound. Furthermore an inversion barrier of 30 kJ mol^{-1} was determined, significantly lower than that in model acyclic amines. In the crystal structure of TMPD,[32] the bond angles around the nitrogen atoms sum up to 353°. In **7c**, the angles around N14 sum up to 349°, whereas those around N4 sum up to 345°, indicating a greater degree of pyramidalization.

Molecular-mechanics (Macromodel v.4.5,[33] MM3* force field) calculations were performed on compound **7a**. Using the Monte Carlo conformational search method, 6 conformers were found within an energy range of 8 kJ mol^{-1}; these are depicted in the first three rows of Figure 5 (A to F). In all these conformers the phenylenediamine chromophore is in the *endo* position. Conformer C shows the closest resemblance to the crystal structure of **7c**. The lowest energy conformer in which the phenylenediamine chromophore is in the *exo* position (G) has a steric energy circa 15 kJ mol^{-1} above the global minimum.

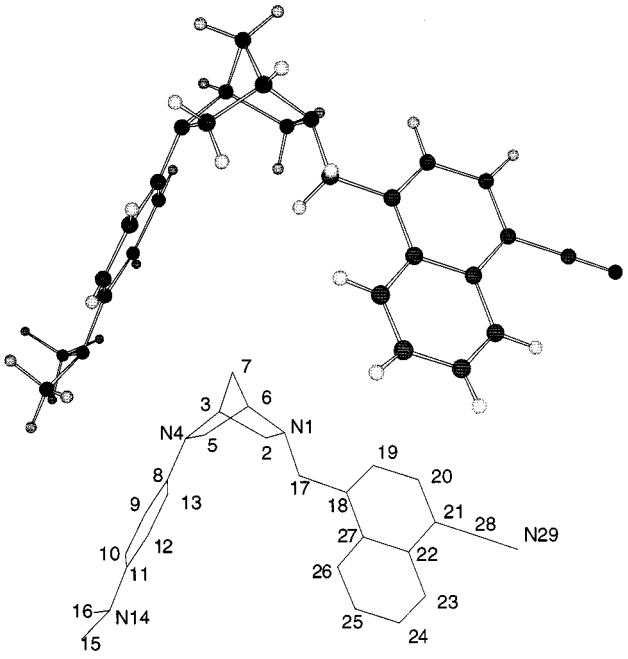

Figure 4. Crystal structure of **7c**; the numbering of the non-hydrogen atoms is shown in the wireframe presentation

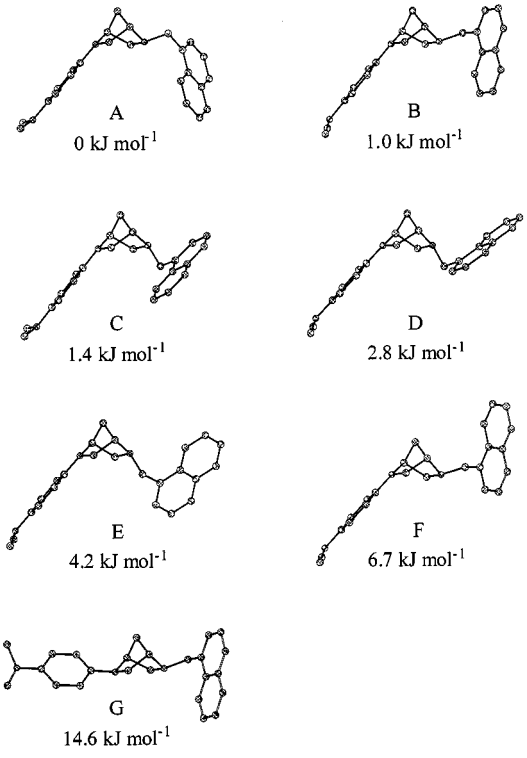

Figure 5. Lowest-energy conformers (A−F) of **7a** (MM3 force field); species G is the lowest-energy conformer in which the naphthylmethyl group adopts the *exo* orientation

Variable-temperature 400-MHz ^{1}H NMR measurements were performed on **7a** in [D_8]toluene. At 225 K, most signals were separated and the proton peaks could be assigned with the aid of C−H HETCOR and NOESY experiments. Relevant intramolecular proton−proton distances in the calculated structures A−G were subsequently measured and checked for presence or absence of a corresponding cross peak in the NOESY spectrum. The predominance of the *endo* configuration in the acceptor unit is supported by the absence of cross peaks between the protons on C7 and those on C19/26 and C17, respectively. When the acceptor is situated in the *exo* position, these distances are always shorter than 3.5 Å. A clear cross peak is observed between the C26 naphthalene proton and the bridgehead proton on C6, which are ca. 4.8 Å apart in the crystal structure. In the calculated conformer E, this H−H distance is 3.1 Å and all other observed NOE effects are also in accordance with the interproton distances in this structure. This indicates that the naphthalene acceptor chromophore is at least not exclusively in the same orientation in solution as it is in the crystal structure.

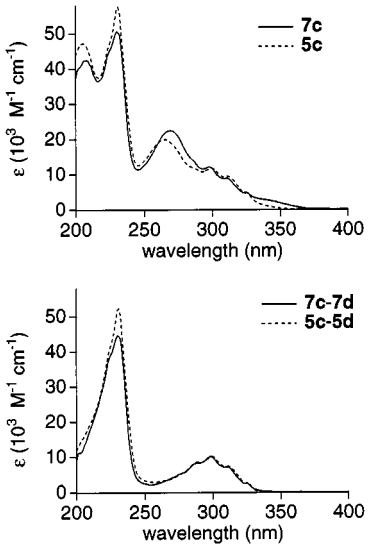

Figure 6. UV-absorption spectra in cyclohexane of compounds **5c** and **7c**, and the difference spectra of **7c** and **7d**, and **5c** and **5d**, respectively

UV-Absorption Spectra of the Donor−Acceptor Compounds

The UV-absorption spectra of **5c** and **7c**, two compounds incorporating the strongest acceptor (cyanonaphthalene), are shown in Figure 6. The spectra consist of the overlapping absorptions of the phenylenediamine and cyanonaphthalene chromophores. This can be convincingly shown by subtraction of the absorptions of the corresponding model donor compounds **5d** and **7d**. The difference spectra, included in Figure 6, are identical to the spectrum of 1-cyano-4-methylnaphthalene. Thus, direct excitation of the (compact) charge-transfer state is not possible even for **7c**, which on the basis of its crystal structure can easily adopt a sandwich-like conformation in which donor and acceptor have π-overlap.

Steady-State Fluorescence of the Donor−Acceptor Compounds

For the six compounds with naphthalene and cyanobenzene as electron acceptors, **5a**−**7a** and **5b**−**7b**, the fluorescence spectra were measured in various solvents. The fluorescence maxima (with the total fluorescence quantum yields in parentheses, including the local fluorescence of the donor) are listed in Table 5. For the **5a**−**7a** and **5b**−**7b** series, the spectra in cyclohexane are given in Figure 7. In both series, the piperidine-bridged systems (**6a** and **6b**) show substantially less quenching of the local fluorescence of the phenylenediamine donor (maximum at 390 nm) than the others do. In the **5a**−**7a** series (naphthalene as electron acceptor), compound **7a** shows the strongest quenching of the local fluorescence, which is in accordance with the lower oxidation potential of the phenylenediamine donor attached to the diazabicycloheptane framework and the fact that the donor−acceptor distance in the ground state is significantly smaller than that in systems **5a** and **6a**. The CT emission of **6a** is largely obscured by the strong local fluorescence. The long-wavelength bands near 500 nm in **5a**, **6a**, and **7a** are attributable to CT fluorescence from conformations in which donor and acceptor are in close contact: this emission resembles that of *inter*molecular exciplexes between TMPD and naphthalene.[34] A similar band was also observed when the fluorescence of solutions containing high concentrations of naphthalene added to donor model compound **5d** was measured. A corresponding CT emission in the series **5b**−**7b** occurs at lower energy ($\lambda_{max} \approx 520$ nm), because of the stronger acceptor involved.

In the other solvents, a decrease in local fluorescence intensity is observed on going to more polar solvents. The same trend can be observed for the two series containing either a naphthalene or cyanobenzene acceptor.

In the case of the piperidine-bridged harpooning compound **1** studied by Wegewijs (see Scheme 1),[3,4,7,35−37] it was convincingly shown that the formation of the compact charge-transfer (CCT) state is preceded by an extended charge-transfer (ECT) species in which the piperidine ring maintains the chair conformation preferred in the ground state. For the compounds studied here, we also observed fluorescence from a species in which donor and acceptor are in close contact. Because of the similarity of **5** and **6** to **1**, we anticipated that the CCT species should be preceded by an ECT species in these compounds too. The predicted fluorescence maxima for the ECT species of compounds **5a**−**b** and **6a**−**b** can be estimated by taking the ECT fluorescence maximum of **1** (circa 384 nm in alkane solvents) as a basis and correcting for the differences in redox potentials. In this way we calculated the expected ECT fluorescence maxima of **5a** and **6a** to be around 372 nm and those of **5b** and **6b** around 400 nm. As we show below, the ECT emission maxima are actually found at substantially lower energies, which may be due to differences in the charge dis-

Table 5. CT fluorescence maxima [nm] of the **5a−7a** and **5b−7b** series in various solvents (the total fluorescence quantum yields are given in parentheses, including the local fluorescence of the donor; excitation wavelength 308 nm)

Solvent	Δf[a]	**5a**	**6a**	**7a**	**5b**	**6b**	**7b**
n-Hexane	0.092	480 (0.03)	[b] (0.09)	484 (0.02)	522 (0.03)	508 (0.06)	532 (0.01)
Cyclohexane	0.100	480 (0.03)	[b] (0.12)	484 (0.02)	522 (0.04)	510 (0.07)	532 (0.01)
Methylcyclohexane	0.100	480 (0.03)	[b] (0.11)	484 (0.02)	522 (0.04)	510 (0.06)	532 (0.01)
Di-*n*-hexyl ether	0.170	503[c]		510[c]			
Di-*n*-pentyl ether	0.171	504 (0.02)	499 (0.04)	514 (0.02)	546 (0.01)	542 (0.01)	558 (0.01)
Di-*n*-butyl ether	0.194	508 (0.01)	500 (0.04)	518 (0.02)	554 (0.01)	543 (< 0.01)	560 (< 0.01)
Di-*n*-propyl ether	0.213	518 (0.01)	506 (0.01)	526 (0.01)	560 (< 0.01)		
Diisopropyl ether	0.237	520 (0.01)	508 (0.01)	528 (0.01)	566 (< 0.01)	550 (< 0.01)	576 (< 0.01)
Diethyl ether	0.251	547 (< 0.01)	532 (0.01)	543 (< 0.01)			
Pentyl acetate	0.259	570 (< 0.01)		568 (< 0.01)			
Benzene	0.116[d]	524 (0.02)	507 (0.04)	538 (0.02)			
Dioxane	0.122[d]	554[c]	528 (0.02)	564[c]			

[a] See Equation (4). − [b] Maximum obscured by strong local emission. − [c] Quantum yield not determined. − [d] Benzene and dioxane are known to behave as more polar than expected on the basis of their Δf value.

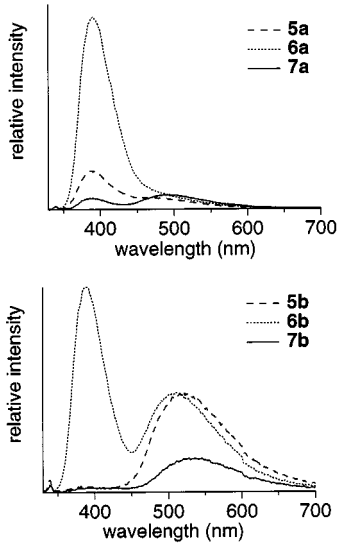

Figure 7. Fluorescence spectra of **5a−7a** (left) and **5b−7b** (right) in cyclohexane, intensities are corrected for the differences in absorbance at the excitation wavelength (308 nm)

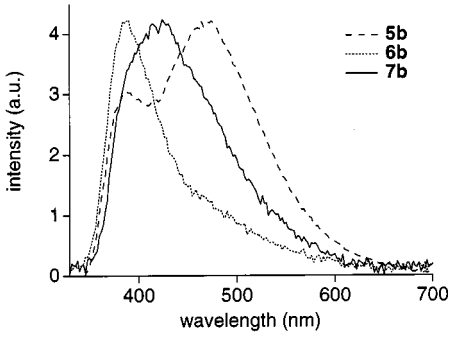

Figure 8. Fluorescence spectra of compounds **5b−7b** in Telene, excitation wavelength 308 nm

tributions and in internal and solvent reorganization energies between the different systems.

The fluorescence spectra of all compounds were also measured in a nonpolar polymer matrix (Telene, see Exp. Sect.). The polarity of this matrix is comparable to that of alkane solvents. For compounds **5a−7a**, a single fluorescence band around 390 nm was observed in the polymer films (spectra not shown). The band around 480 nm, which had been observed in liquid alkanes and attributed to the CCT species, is absent. Clearly, the species in which donor and acceptor are in close contact cannot be formed in the rigid polymer matrix.

The spectra of compounds **5b−7b**, scaled to the same intensity, are shown in Figure 8. Compounds **5b** and **6b** clearly show a band around 390 nm, probably local fluorescence from the phenylenediamine donor chromophore. Compound **5b** shows an additional band around 470 nm. It is tempting to ascribe this band to fluorescence from an ECT species, although the difference between the position of this band and the CCT emission band, observed in cyclohexane at 522 nm, is rather small. For **6b**, a broad CT-type fluorescence band also seems to be present, slightly red-shifted in comparison to the local fluorescence. However, the maximum of this emission band cannot be resolved properly. Compound **7b** shows a broad emission spectrum. The band around 530 nm in the alkane solvents, ascribed to emission from a CCT state, seems to have largely disappeared, however.

Temperature Dependence of Fluorescence

With all compounds, fluorescence in methylcyclohexane was studied as a function of temperature. On lowering the temperature, the compounds with the naphthalene acceptor − **5a**, **6a**, and **7a** − show an increase in the local emission around 390 nm, concomitantly with a decrease in the long wavelength CT emission situated around 480 nm (spectra not shown). At 147 K, the temperature at which methylcyclohexane forms a glass, the spectra of **5a** and **6a** are similar to the fluorescence spectra of the corresponding model donor systems **5d** and **6d**. This implies that the electron

transfer rate is very slow at low temperatures. In the spectrum of **7a** at 147 K, a shoulder on the red side of the 390 nm band is clearly observable, indicating that, in this compound, a charge-transfer state can still be populated. At still lower temperatures (circa 120 K), phosphorescence of the naphthalene chromophore is observed.

The spectra at different temperatures of the compounds with the stronger cyanobenzene acceptor − **5b**, **6b**, and **7b** −are displayed in Figure 9. Compound **5b** shows a moderate shift of the CT emission band to shorter wavelength upon cooling, but no local fluorescence appears even at the lowest temperature, which indicates that electron transfer has a very low activation barrier in this system. The intensity of the emission band increases at first, but decreases again from 173 K to 147 K. At 147 K, a maximum at around 480 nm is observed, close to the value found in the polymer matrix. We tentatively attribute this emission to an ECT species. For **6b**, it is more difficult to identify the changes that are taking place. A slight increase in the local emission around 390 nm is observed upon cooling. The change in the shape of the spectrum below 173 K suggests that an additional band is appearing in the 400−450-nm region. For **7b**, which − like **5b** − is devoid of local fluorescence, the appearance of a new fluorescence band at ca. 460 nm can clearly be seen.

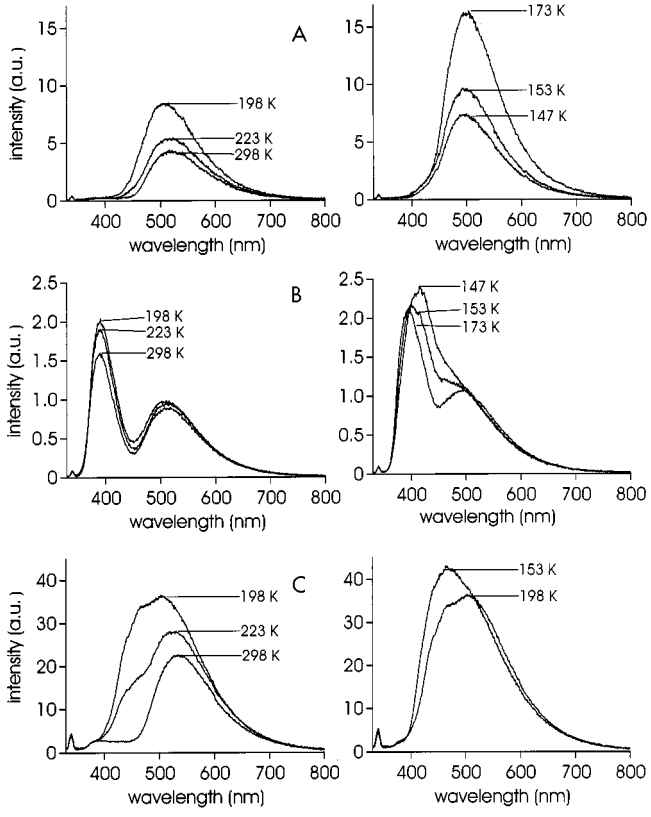

Figure 9. Fluorescence spectra of **5b** (A), **6b** (B), and **7b** (C) in methylcyclohexane at different temperatures, excitation wavelength 308 nm

It is hard to relate the dependence of fluorescence on mobility and temperature to the conformational processes that take place in these compounds. A complicating factor in these systems is the low-lying, locally excited state of the phenylenediamine chromophore, which hampers observation of the extended charge-transfer species. In the next section we present time-resolved fluorescence measurements to provide more convincing evidence for the involvement of this intermediate ECT state in the formation of the CCT species.

Fluorescence Kinetics of the Donor−Acceptor Compounds: 5a at Room Temperature in Cyclohexane

The fluorescence decays of the donor−bridge−acceptor compounds **5a**, **6a**, and **7a** were measured in cyclohexane at multiple wavelengths, using a streak camera system and the single-photon counting technique (SPC). We describe the streak camera results obtained for **5a** in detail. The SPC results are in good agreement with these, and are given in the Supporting Information.

Three decay times were necessary in order to obtain satisfactory fits. In Figure 10 we show two representative decay traces, together with the global fit. In general, the uncertainties in the estimated rate constants are 10% or less.

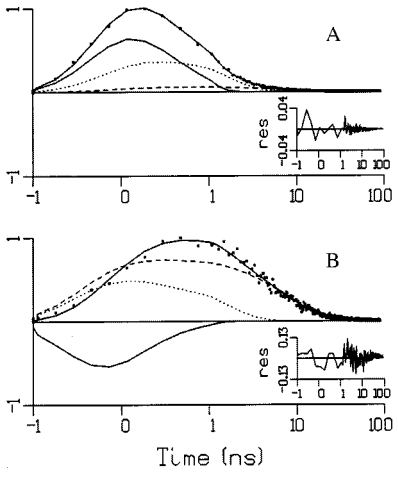

Figure 10. Representative traces (A: 395 nm; B: 507 nm) of fluorescence intensity versus time and global fits from streak camera measurements for **5a** in cyclohexane; insets show residuals of a fit with three monoexponential decays; the sum of the contributions is represented by a solid line through the measured points. Time constants 0.29, 1.33, and 7.9 ns (solid, dotted, and dashed lines, respectively); the time base is linear around the maximum of instrument response and logarithmic from 1 to 100 ns

The fitted decay times of 0.29, 1.33, and 7.9 ns are attributed to the involvement of the locally excited (LE) state of the phenylenediamine electron donor, an ECT species, and the CCT species, respectively. This is the first clear experimental evidence that an ECT intermediate is indeed involved in the formation of the CCT species in **5a**. The decay-associated spectra (DAS) are shown in Figure 11.

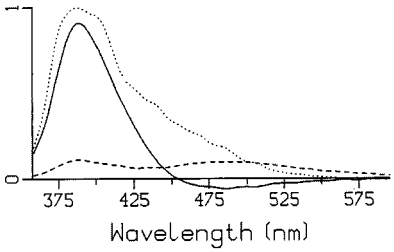

Figure 11. Decay-associated spectra (DAS) of **5a** in cyclohexane; time constants 0.29, 1.33, and 7.9 ns (solid, dotted, and dashed lines, respectively); to facilitate comparison, the DAS of the fastest decaying component has been divided by five

The negative amplitude of the LE state at longer wavelengths indicates that it is a precursor for the other species. We subsequently assumed a sequential model with increasing lifetimes for the kinetics − i.e., LE → ECT → CCT − to estimate the species-associated spectra (SAS). The first SAS [solid in Figure 12 and Figure S2 (Supporting Information)] represents the emission spectrum at time zero and is attributed to the LE state. After 0.3 ns, this first SAS is replaced by the second SAS (dotted), which possesses a shoulder near 470 nm that we attribute to the ECT species. This second SAS is in turn replaced after 1.3 ns by the third SAS (dashed), which displays a second peak, attributable to the CCT species, at 500 nm. The fact that the second and third SASs still possess peaks near 390 nm indicates that they also contain emissions from the LE state. Thus, the SASs obtained in this way indicate that equilibria exist between the three species.

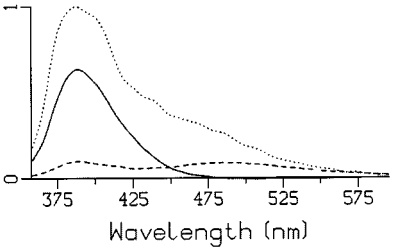

Figure 12. Species-associated spectra (SAS) of **5a** in cyclohexane; resulting from an analysis with a sequential model with increasing time constants of 0.29, 1.33, and 7.9 ns (solid, dotted, and dashed, respectively); scaling of SAS assumes that the ensemble LE/ECT/CCT decays exclusively by CCT; to facilitate comparison, the SAS of the LE component has been divided by ten

An equilibrium model to fit the data was therefore applied (Figure 13). In order to estimate the rate constants, the ECT and CCT components are assumed not to emit below 390 nm, and thus their SAS are zero below 390 nm. The shape of the decay below 390 nm is described by three lifetimes and two relative amplitudes and contains all information needed to estimate the five forward and backward rate constants. When we now estimate the SAS, the spectra shown in Figure 14 are obtained.

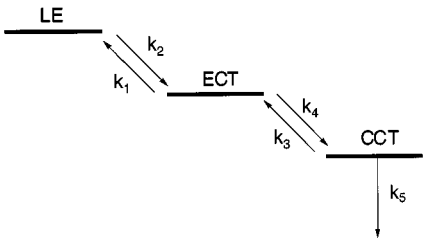

Figure 13. Equilibrium model to fit the decay traces of **5a** in cyclohexane; decay of the LE state and of the ECT state by fluorescence or nonradiative decay (other than electron transfer) may occur, but this is not distinguishable in the kinetic experiment

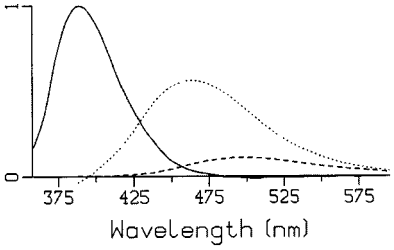

Figure 14. Species-Associated Spectra (SAS) of **5a** in cyclohexane produced by an analysis using an equilibrium model: LE ⇄ ECT ⇄ CCT (respectively: solid, dotted, and dashed); in order to estimate the rate constants, the ECT and CCT components are assumed not to emit below 390 nm, and thus their SAS are zero below 390 nm; scaling of SAS assumes that the ensemble LE/ECT/CCT decays exclusively by CCT; to facilitate comparison, the SAS of the LE component has been divided by ten

The observed spectra corroborate our assignment of the decay times to the different species. The locally excited state of the phenylenediamine electron donor fluoresces around 390 nm and is largely quenched because of electron transfer. From the locally excited state, a CT species with a maximum at ca. 470 nm is formed. This is probably the ECT state, which is in equilibrium with the locally excited state. Around 500 nm we observe the CCT species, which in turn is in equilibrium with the ECT species. The ECT species has its maximum at rather long wavelength. For compound **5b**, however, we observed a fluorescent species at ca. 470 nm both in a rigid polymer matrix and in methylcyclohexane at low temperature, media in which the formation of a CCT state is severely hindered.

Solvent Dependence of the Fluorescence of 5a, 6a, and 7a

The fluorescence of **5a**, **6a**, and **7a** was measured with the streak camera system in a series of solvents. Three components were needed to model the decay traces. For compounds **6a** and **7a** in cyclohexane, SPC data were also obtained; four spectrally and temporally distinct components are needed to describe these. This indicates that, although the streak camera data give a satisfactory picture of the photophysical behavior of the compounds in terms of three species, the situation may in fact be more complex, due, for example, to the involvement of slightly different conformations of the LE or ECT species. For **5a** in all solvents, the kinetics were fitted to the model of Figure 13, in which

Table 6. Estimated emission maxima of the different species of **5a**, **6a**, and **7a** in various solvents, obtained from analysis of the streak images (excitation wavelength 337 nm)

Solvent	Δf	**5a**[a] LE	ECT	CCT	**6a**[a] LE	ECT	CCT	**7a**[a] LE	CT1	CT2
Methylcyclohexane	0.100	25.2	21.6	20.2	24.8	24.7	20.0	24.8	20.0	19.9
Cyclohexane	0.100	25.0	21.4	19.7	25.0	25.0	19.6	24.9	19.9	19.7
trans-Decalin	0.110	25.0	21.1	19.7	24.7	24.0	19.8	25.1	20.0	19.9
Di-*n*-pentyl ether	0.171	24.9	19.2	19.1	24.8	20.4	19.1	24.9	19.0	18.9
Benzene	–	24.1	18.6	18.4	–	–	–	–	–	–
Diisopropyl ether	0.237	25.0	18.8	18.5	24.8	19.3	18.8	25.0	18.5	18.4
Diethyl ether	0.251	24.9	18.2	18.0	24.7	18.6	18.4	24.9	18.1	18.1

[a] Emission maximum ν_{max} (10^3 cm^{-1}) as defined in Equation (2).

Table 7. Estimated decay times (ns; estimated uncertainties < 10%) for **5a**–**7a** in various solvents, obtained from analysis of the streak images

Solvent	Δf	**5a** τ_1	τ_2	τ_3	**6a** τ_1	τ_2	τ_3	**7a** τ_1	τ_2	τ_3
Methylcyclohexane	0.100	0.35	2.0	11	0.37	3.1	31	0.30	2.6	17
Cyclohexane	0.100	0.34	1.7	9.2	1.1	2.8	31	0.30	7.6	20
trans-Decalin	0.110	0.32	2.5	11	0.90	3.0	13	0.28	2.1	17
Di-*n*-pentyl ether	0.171	0.16	3.2	16	0.21	4.4	40	0.17	4.6	25
Benzene	–	0.16	4.8	22	–	–	–	–	–	–
Diisopropyl ether	0.237	0.14	3.8	28	0.14	4.9	51	0.17	5.0	27
Diethyl ether	0.251	0.08	15	33	0.21	11	52	0.22	5.9	26

equilibria are invoked both between the locally excited state and the ECT state and between the ECT state and the CCT state. For **6a** and **7a**, equilibria were also necessary in most cases in order to obtain reasonable SAS. This yields the emission maxima given in Table 6 and the decay times as presented in Table 7. The experimental parameters to fit the emission spectra and the rate constants describing the equilibrium model for **5a** are given in Tables 8 and 9, respectively. The fluorescence spectra were fitted with the model function given in Equation (2).

$$\varepsilon(\nu) = \nu^5 f_{max} \exp(-\ln 2[\ln(1+2b(\nu-\nu_{max})/\Delta\nu)/b]^2) \quad (2)$$

Note that, with the skewness parameter $b \rightarrow 0$, the exponent in Equation (2) reduces to a Gaussian. The shape described by this model function is indistinguishable from the spectral shape predicted for CT-type emission bands.[38]

As can be seen for **5a**, the emission maximum of the locally excited state hardly changes upon increasing the solvent polarity, but a significant decrease in its decay time is observed, due to the electron transfer process yielding the ECT species. On increasing the solvent polarity, this ECT species shows a red shift, together with an increase in the decay time. The red shift, concomitant with an increase in the CCT decay time, is observed for the CCT species as well, with increasing solvent polarity (Table 7).

If we study the rate constants and the free energy differences calculated from them (see Table 8) (under the assumption that the LE/ECT/CCT ensemble decays exclusively through CCT), the following conclusions can be drawn. On increasing the solvent polarity, the free energy difference between the locally excited state and the ECT state increases as expected. This is also evident from the increasing difference between the emission maxima of the LE and ECT species on going to more polar solvents. In the calcu-

Table 8. Estimated rate constants [10^9 s^{-1}] (estimated uncertainties < 10%) for **5a** in various solvents at room temperature and free energy differences [kJ mol^{-1}], calculated using the kinetic scheme of Figure 13

Solvent	k_1	k_2	k_3	k_4	k_5	ΔG_{LE-ECT}	$\Delta G_{ECT-CCT}$
Methylcyclohexane	0.372	2.4	0.034	0.56	0.098	−4.6	−7.0
Cyclohexane	0.374	2.5	0.053	0.65	0.12	−4.7	−6.2
trans-Decalin	0.275	2.8	0.025	0.42	0.10	−5.8	−6.9
Di-*n*-pentyl ether	0.087	6.1	0.041	0.26	0.077	−10.5	−4.6
Benzene	0.089	6.0	0.017	0.19	0.050	−10.4	−6.0
Diisopropyl ether	0.029	7.1	0.018	0.25	0.039	−13.6	−6.5
Diethyl ether	0.005	13	0.002	0.064	0.032	−19.5	−9.0

lated free energy difference between the ECT and CCT species, no clear trend can be discerned. It would be expected that this difference would decrease, due to the relatively greater stabilization of the ECT species with increasing solvent polarity, relative to that of the CCT species. This shows up in, for example, the decreasing difference between the energies of the ECT and CCT emission maxima (Table 6). Perhaps the assumption that the ECT→CCT conversion takes place quantitatively is incorrect, and the ECT species also decays by other pathways, such as intersystem crossing to a local triplet state. This becomes more significant in more polar solvent as the folding rate k_4 decreases.

For **6a** and **7a**, the emission maximum of the shortest living component also lies at approximately the same wavelength in all solvents, and is attributable to emission from the locally excited state. For **6a**, the second component is attributable to an ECT species. In alkane solvents its fluorescence maximum is approximately the same as that of the LE species, as can be concluded from Table 6. We had already anticipated that the maximum of the ECT species should be fairly close to that of the locally excited state of the phenylenediamine electron donor. The position of the CCT species is comparable to that of compound **5a**. Compound **7a** also shows two CT species, but at approximately the same wavenumber. Given the crystal structure of **7a** and the molecular mechanics calculations discussed earlier, we cannot really speak of ECT and CCT species in this compound. The similar maxima indicate that no large differences in the donor−acceptor distance exist in the two CT species.

The solvent dependence of charge-transfer fluorescence can be analyzed on the basis of dielectric continuum theory, using the well known Lippert−Mataga Equation (3).[39,40] In this equation, the solvent dependence of the charge-transfer emission wavenumber ν_{CT} correlates with the solvent polarity parameter Δf [Equation (4)], where $\nu_{CT}(0)$ [cm^{-1}] is the emission maximum in the gas phase, μ_{CT} [Debye] is the dipole moment of the charge-transfer state, h is Planck's constant, c is the velocity of light, ρ [Å] is the effective radius of the solvent cavity occupied by the molecule, ε_s is the solvent dielectric constant, and n is its refractive index.

$$\nu_{CT} = \nu_{CT}(0) - \frac{2\mu_{CT}^2}{hc\rho^3}\Delta f = \nu_{CT}(0) - 10070\frac{\mu_{CT}^2}{\rho^3}\Delta f \quad (3)$$

$$\Delta f = \frac{(\varepsilon_s - 1)}{(2\varepsilon_s + 1)} - \frac{(n^2 - 1)}{(4n^2 + 2)} \quad (4)$$

If we plot the emission maxima of the various CT species versus the corresponding solvent polarity parameters Δf, the Lippert−Mataga plots shown in Figure 15 are obtained. As can be seen, the CT maxima can be fitted reasonably well by linear relationships. The values obtained from this analysis are given in Table 9. For **5a** and **6a**, the slopes obtained for the CCT species are indicative of a species with a relatively small dipole moment (around 13 Debye if a cavity radius of 5.4 Å is assumed). This holds equally for both CT species of **7a**. The slope for the ECT species of **5a** is rather small compared to previously studied piperidine-bridged harpooning compounds **1** and compound **6a**. It seems likely that the negative charge on the acceptor plays a role in polarizing the ECT state in **5a** in such a way that, even in the presence of the very strong phenylenediamine donor, the positive charge remains partly on the trialkyl-substituted nitrogen atom. As observed previously, weaker donors than the phenylenediamine unit result in a situation in which the positive charge is mainly localized on that trialkyl-substituted nitrogen atom.[8] In these cases, harpooning is prevented because the electrostatic driving force is absent, but in **5a** there is sufficient charge on the aromatic donor to allow the folding process. In the CCT species, the positive charge is definitely on the phenylenediamine unit.

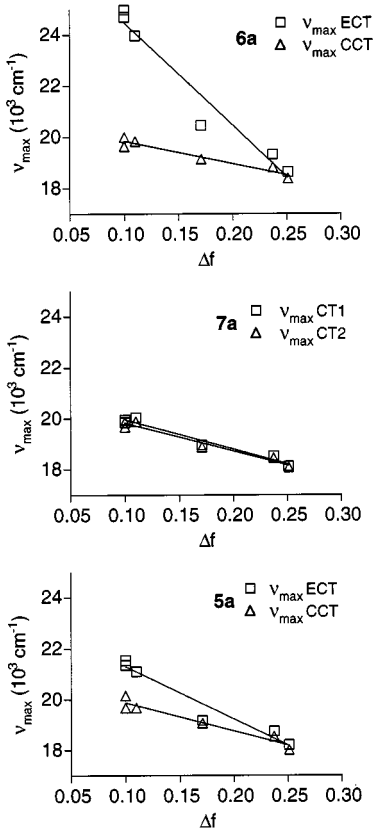

Figure 15. Lippert−Mataga plots for **5a**, **6a**, and **7a**

Table 9. Experimental parameters [10^3 cm^{-1}] for **5a**−**7a** obtained from Lippert−Mataga analysis [Equations (3) and (4)]

Compound	Species	$2\mu^2/hc\rho^3$	$h\nu_{CT}(0)$
5a	ECT	20.8 ± 2.5	23.4 ± 0.4
	CCT	11.2 ± 1.5	21.0 ± 0.3
6a	ECT	40.3 ± 4.4	28.5 ± 0.8
	CCT	8.8 ± 1.2	20.7 ± 0.2
7a	CT1	11.7 ± 1.1	21.1 ± 0.2
	CT2	11.1 ± 1.1	20.9 ± 0.2

Conclusion

Study of the different phenylenediamine donor compounds demonstrates the importance of choosing appropriate model chromophores. It has been shown that the remarkable differences between these compounds can largely be traced back to differences in molecular geometries of the phenylenediamine chromophores.

With the available data on the model donor compounds, it is possible to perform a proper comparison of the different semiflexibly and rigidly bridged systems. No evidence for ground-state interaction between the donor and acceptor was found, implying that the charge-transfer states formed in these compounds are populated by excitation to the locally excited state of the donor and/or acceptor. The charge-transfer fluorescence observed for the donor−acceptor systems in nonpolar solvents is attributable to species in which donor and acceptor are in close contact (CCT). In rigid or very viscous media (polymer matrix or methylcyclohexane at low temperature), the emission attributed to the CCT species is not present. Under these conditions, emission bands that must stem from ECT-type species are observed for the compounds with the cyanophenyl acceptor − **5b**, **6b**, and **7b** − but the steady-state spectra do not allow accurate determination of band maxima.

For the piperidine and piperazine compounds **5a** and **6a**, time-resolved fluorescence measurements provide clear evidence for the involvement of ECT species. For **7a**, the presence of two similar CT species, with relatively small charge separation distances, can be inferred.

The spectrotemporal analysis of the fluorescence of **5a** demonstrates the presence of equilibria between the different excited state species, and has allowed the free energy differences between them to be estimated. With increasing solvent polarity, the ECT state is strongly stabilized relative to the LE state, but the difference between ECT and CCT does not appear to decrease as expected. Although this may in part be due to the assumptions made in our analysis, it should be noted that the analysis of the solvatochromic shifts of the fluorescence maxima indicates that the ECT species in compound **5a** still has some charge density on the trialkyl-substituted nitrogen atom, which reduces the electrostatic interaction that triggers the harpooning process. The tendency to delocalize positive charge over the two nitrogen atoms in a piperazine ring is very strong.

Experimental Section

Single-Crystal X-ray Structure Determination of Compound 7c: Orthorhombic crystals, $P2_12_12_1$, a = 7.893(2), b = 8.919(2), c = 30.342(5) Å, V = 2136.0(8) Å^3, Z = 4, D_x = 1.13 gcm^{-3}, λ(Mo-K_α) = 0.71069 Å, μ(Mo-K_α)=0.64 cm^{-1}, F(000) = 736, room temperature. Final R = 0.052 for 1625 observed reflections. A crystal with dimensions approximately 0.40 × 0.65 × 0.70 mm was used for data collection with an Enraf−Nonius CAD-4 diffractometer with graphite-monochromated Mo-K_α radiation and ω-2θ scan. A total of 3525 unique reflections were measured within the range $0 \le h \le 11$, $0 \le k \le 12$, $0 \le l \le 42$. Of these, 1625 were above the significance level of 2.5 σ(I). The maximum value of sin(θ)/λ was 0.70 Å^{-1}. Two reference reflections (032, 308) were measured hourly and showed no decrease during the 49 h of collecting time. In addition, some 60 "Friedel" reflections were measured and used in the determination of the absolute configuration of the compound. Unit cell parameters were refined by a least-squares fitting procedure, using 23 reflections with $40° < 2\theta < 44°$. Corrections for Lorentz and polarization effects were applied. The structure was solved by the CRUNCH program package.[41] The hydrogen atoms were calculated. Full-matrix, least-squares refinement on F, anisotropic for the non-hydrogen atoms and isotropic for the hydrogen atoms restraining the latter in such a way that the distance to their carrier remained constant at approximately 1.0 Å, converged to R = 0.052, R_w = 0.046, $(\Delta/\sigma)_{max}$ = 0.11, S = 0.279(6). A weighting scheme $w = \{10.5 + 0.011\cdot[\sigma(F_{obs})]^2 + 0.0002/[\sigma(F_{obs})]\}^{-1}$ was used. The secondary isotropic extinction coefficient[33] refined to Ext = 0.42(7). The absolute structure parameter[42] refined to Xabs = 0, thus confirming the correct enantiomer. A final difference Fourier map revealed a residual electron density between −0.1 and 0.1 eÅ^{-3}. Scattering factors were taken from Cromer and Mann.[43,44] All calculations were performed with XTAL,[45] unless stated otherwise. The structure is shown in Figure 4. Bond lengths and bond angles are reported in Tables S1 and S2 (Supporting Information).

Electrochemistry: Cyclic voltammetry measurements were performed using an EG&G Model 273 potentiostat at a scan rate of 50 mV s^{-1}. Solutions of circa 2 mM in acetonitrile (Acros p.A. grade, distilled from calcium hydride) were used, 0.1 M tetrabutylammonium hexafluorophosphate (Fluka, electrochemical grade) being present as supporting electrolyte. Redox potentials were measured relative to the $Ag/AgNO_3$ (0.01 M) system and were referenced to SCE by measuring the oxidation potential of the $FeCp_2/FeCp_2^{+\cdot}$ couple. Since, for the $FeCp_2/FeCp_2^{+\cdot}$ couple, we measured $E^{ox}_{1/2}$ 0.05 V versus $Ag/AgNO_3$ and a value of 0.45 V versus SCE has been reported in the literature[25] for this couple, a value of 0.40 V has been added to our values to reference to SCE.

Spectroscopic Measurements: Electronic absorption measurements were performed with a Hewlett−Packard 8453 diode array spectrometer or a Cary 3E (Varian) spectrophotometer. Molar absorption coefficients were determined using concentrations of 10^{-4}−10^{-5} M. Commercially available spectrograde solvents were used. − Telene OP 2000x (BFGoodrich Company) was obtained as a generous gift from G. W. Buning (Philips Research Laboratories). Telene is a hydrocarbon polymer consisting of [2.2.1]bicycloheptane units. The polymer films were prepared by dissolving the polymer beads and a small amount of the donor−acceptor compound in spectrograde toluene (Aldrich). After spontaneous evaporation of the solvent (at ambient temperature and pressure), the polymer films were dried in a vacuum desiccator. − Fluorescence spectra were recorded with a Spex Fluorolog II emission spectrometer, using an RCA-C31034 GaAs photomultiplier as detector. Spectra were corrected for the wavelength-dependent response of the detection system with the aid of an in-house correction file. Fluorescence quantum yields were determined relative to a reference solution [anthracene in cyclohexane (φ = 0.18) or quinine bisulfate in 1 N sulfuric acid (φ = 0.546)][46] and corrected for the refractive index of the solvent. The samples were made with an absorbance between 0.1 and 0.2 at the excitation wavelength and were deoxygenated by purging with argon for 10−15 min. Commercially available spectrograde solvents were used (Merck, Uvasol), except for di-*n*-butyl ether

(Merck, > 99%, washed three times with sulfuric acid). When the purity of the solvent was found to be insufficient, the solvent was purified by standard procedures. All alkyl ethers were distilled from CaH_2 or $LiAlH_4$ prior to use. All acetates were washed with a saturated sodium carbonate solution and distilled from CaH_2. − Fluorescence measurements at low temperature were performed using an Oxford Instruments liquid nitrogen cryostat DN 1704 with an ITC4 control unit. The samples were degassed using at least four freeze-pump-thaw cycles. Each sample was allowed to equilibrate thermally for at least 20 min prior to data collection. − Fluorescence decay curves at single wavelengths were measured by picosecond time-correlated single-photon counting (SPC). The experimental set-up has been fully described elsewhere.[47] A mode-locked argon-ion laser (Coherent 486 AS Mode Locker and Coherent Innova 200 laser) was used to pump a DCM dye-laser (Coherent model 700) synchronously. The output frequency was doubled with a BBO crystal, resulting in 310−320-nm pulses. A Hamamatsu microchannel plate photomultiplier (R3809) was used as detector. The response function [full width at half maximum (fwhm) ≈ 18 ps] was obtained by monitoring the Raman band of a cell filled with spectrograde water. The cells were painted black with camera varnish on two adjacent sides to avoid reflection at the quartz/air boundary. − The 2D time-resolved fluorescence measurements were performed using a Hamamatsu streak camera system, consisting of a Chromex IS250 spectrograph, an M5677 slow-speed sweep unit, a C4792 trigger unit, a C5680 blanking unit, and a C4742-95 digital CCD camera. For excitation, an LTB MSG400 nitrogen laser (337 nm, fwhm ≈ 0.5 ns) operating at 50 Hz was used (fwhm ≈ 0.5 ns). The excitation and emission light were fiber-coupled to the spectrograph. The images consist of 512 × 512 pixels. In the time direction, the resolution is limited by the width of the excitation pulse (fwhm ≈ 500 ps) and by the pointspread function of the imaging device. Thus, the Gaussian shaped fwhm of the instrument response depends upon the time base used, which varied from fwhm = 0.5 to 5 ns. In the wavelength direction, the resolution is limited by the slit and the grating used and was fwhm ≈ 6 nm. We reduced the number of data points for the analysis by summing the response over 11−13 pixels (depending on the spectral window used), which is effectively a smoothing over circa 7−8 nm. Thus, a data set of 512 × 33 points was routinely used in the further analysis.

Syntheses: Details of the syntheses and characterizations of the compounds studied are provided in the Supporting Information.

Supporting Information: Details of syntheses and characterization, X-ray structural data of compound **7c**, comparison of SPC and streak-camera measurements of **5a** in cyclohexane, estimated spectral and kinetic parameters of **5a**, **6a**, and **7a** in various solvents, as derived from the streak-camera experiments (see also footnote on the first page of this article).

Acknowledgments

We thank Bregje van den Berg and Dr. Jurriaan Zwier for the synthesis of and measurements on compound **6d**. Prof. Dr. L.W. Jenneskens (Utrecht University) is gratefully acknowledged for use of his cyclic voltammetry apparatus. This work was supported by the Netherlands Organization for Scientific Research (Nederlandse Organisatie voor Wetenschappelijk Onderzoek, NWO).

[1] J. W. Verhoeven, in: *Electron transfer − from isolated molecules to biomolecules*, part 1, vol. 106 (Eds.: J. Jortner, M. Bixon), Wiley, New York, **1999**, pp. 603.
[2] M. Polanyi, *Atomic Reactions*, Williams and Nordgate, London, **1932**.
[3] B. Wegewijs, R. M. Hermant, J. W. Verhoeven, A. G. M. Kunst, R. P. H. Rettschnick, *Chem. Phys. Lett.* **1987**, *140*, 587.
[4] B. Wegewijs, R. M. Hermant, J. W. Verhoeven, M. P. de Haas, J. M. Warman, *Chem. Phys. Lett.* **1990**, *168*, 185.
[5] I. H. M. Van Stokkum, T. Scherer, A. M. Brouwer, J. W. Verhoeven, *J. Phys. Chem.* **1994**, *98*, 852.
[6] T. Scherer, I. H. M. van Stokkum, A. M. Brouwer, J. W. Verhoeven, *J. Phys. Chem.* **1994**, *98*, 10539.
[7] B. Wegewijs, J. W. Verhoeven, in: *Electron transfer − from isolated molecules to biomolecules*, part 1, vol. 106 (Eds.: J. Jortner, M. Bixon), Wiley, New York, **1999**, pp. 221.
[8] X. Y. Lauteslager, B. Wegewijs, J. W. Verhoeven, A. M. Brouwer, *J. Photochem. Photobiol. A* **1996**, *98*, 121.
[9] G. F. Mes, H. J. van Ramesdonk, J. W. Verhoeven, *J. Am. Chem. Soc.* **1984**, *106*, 1335.
[10] X. Y. Lauteslager, M. J. Bartels, J. J. Piet, J. M. Warman, J. W. Verhoeven, A. M. Brouwer, *Eur. J. Org. Chem.* **1998**, 2467.
[11] R. J. Willemse, J. J. Piet, J. M. Warman, F. Hartl, J. W. Verhoeven, A. M. Brouwer, *J. Am. Chem. Soc.* **2000**, *122*, 3721.
[12] A. M. Brouwer, J. M. Zwier, C. Svendsen, O. S. Mortensen, F. W. Langkilde, R. Wilbrandt, *J. Am. Chem. Soc.* **1998**, *120*, 3748.
[13] A. M. Brouwer, P. G. Wiering, J. M. Zwier, F. W. Langkilde, R. Wilbrandt, *Acta Chem. Scand.* **1997**, *51*, 217.
[14] J. M. Zwier, Ph.D. thesis, University of Amsterdam, **2000**.
[15] J. M. Zwier, A. M. Brouwer, G. Balakrishnan, T. Keszthelyi, J. F. Offersgaard, R. Wilbrandt, manuscript in preparation.
[16] J. L. de Boer, A. Vos, *Acta Crystallogr., Sect. B* **1972**, *28*, 835.
[17] J. L. de Boer, A. Vos, *Acta Crystallogr., Sect. B* **1972**, *28*, 839.
[18] L. Meites, P. Zuman, *CRC Handbook Series in Organic Electrochemistry*, CRC Press, Cleveland OH, **1976**.
[19] E. C. Taylor, *Synthesis* **1981**, 606.
[20] A. Nose, T. Kudo, *Chem. Pharm. Bull.* **1981**, *29*, 1159.
[21] A. G. Giumanini, G. Chiavara, M. M. Musiani, P. Rossi, *Synthesis* **1980**, 743.
[22] T. Scherer, W. Hielkema, B. Krijnen, R. M. Hermant, C. Eijckelhoff, F. Kerkhof, A. K. F. Ng, R. Verleg, E. B. van der Tol, A. M. Brouwer, J. W. Verhoeven, *Recl. Trav. Chim. Pays-Bas* **1993**, *112*, 535.
[23] G. Gritzner, J. Kuta, *Pure Appl. Chem.* **1984**, *56*, 461.
[24] R. R. Gagné, C. L. Koval, G. C. Lisensky, *Inorg. Chem.* **1980**, *19*, 2855.
[25] W. C. Barette, Jr., H. W. Johnson, Jr., D. T. Sawyer, *Anal. Chem.* **1984**, *56*, 1890.
[26] A. M. Brouwer, *J. Phys. Chem. A* **1997**, *101*, 3626.
[27] J. M. Zwier, J. Wichers Hoeth, A. M. Brouwer, *J. Org. Chem.* **2001**, *66*, 466.
[28] A. D. Becke, *J. Chem. Phys.* **1993**, *98*, 5648.
[29] M. J. Frisch, G. W. Trucks, H. B. Schlegel, P. M. W. Gill, B. G. Johnson, M. A. Robb, J. R. Cheeseman, T. Keith, G. A. Petersson, J. A. Montgomery, K. Raghavachari, M. A. Al-Laham, V. G. Zakrzewski, J. V. Ortiz, J. B. Foresman, J. Cioslowski, B. B. Stefanov, A. Nanayakkara, M. Challacombe, C. Y. Peng, P. Y. Ayala, W. Chen, M. W. Wong, J. L. Andres, E. S. Replogle, R. Gomperts, R. L. Martin, D. J. Fox, J. S. Binkley, D. J. Defrees, J. Baker, J. J. P. Stewart, M. Head-Gordon, C. Gonzalez, J. A. Pople, *Gaussian 94, Revision B.2*, Pittsburgh PA, **1995**.
[30] R. E. Stratmann, G. E. Scuseria, M. J. Frisch, *J. Chem. Phys.* **1998**, *109*, 8218.
[31] D. A. Forsyth, W. Zhang, J. A. Hanley, *J. Org. Chem.* **1996**, *61*, 1284.
[32] I. Ikemoto, G. Katagiri, S. Nishimura, K. Yakushi, H. Kurado, *Acta Crystallogr., Sect. B* **1979**, *35*, 2264.
[33] F. Mohamadi, N. G. J. Richards, W. C. Guida, R. Liskamp, M. Lipton, C. Caufield, G. Chang, T. Hendrickson, W. C. Still, *J. Comput. Chem.* **1990**, *11*, 440.

[34] K. A. Zachariasse, Ph.D. Thesis, Vrije Universiteit Amsterdam, **1972**.
[35] B. Wegewijs, A. K. F. Ng, R. P. H. Rettschnick, J. W. Verhoeven, *Chem. Phys. Lett.* **1992**, *200*, 357.
[36] B. Wegewijs, T. Scherer, R. P. H. Rettschnick, J. W. Verhoeven, *Chem. Phys.* **1993**, *176*, 349.
[37] B. Wegewijs, J. W. Verhoeven, S. E. Braslavsky, *J. Phys. Chem.* **1996**, *100*, 8890.
[38] R. A. Marcus, *J. Phys. Chem.* **1989**, *93*, 3078.
[39] E. Lippert, *Z. Naturforsch., Teil A* **1955**, *10A*, 541.
[40] N. Mataga, Y. Kaifu, M. Koizumi, *Bull. Chem. Soc. Jpn.* **1956**, *29*, 465.
[41] R. de Gelder, R. A. G. de Graaff, H. Schenk, *Acta Crystallogr., Sect. A* **1993**, *49*, 287.
[42] H. D. Flack, *Acta Crystallogr., Sect. A* **1983**, *46*, 688.
[43] D. T. Cromer, J. B. Mann, *Acta Crystallogr., Sect. A* **1968**, *24*, 321.
[44] *International Tables for X-ray Crystallography*, vol. IV, Kynoch Press, Birmingham, **1974**.
[45] S. R. Hall, H. D. Flack, J. M. Stewart, *XTAL 3.2*, **1992**.
[46] S. L. Murov, I. Carmichael, G. L. Hug, *Handbook of Photochemistry*, 2nd ed., Marcel Dekker, Inc., New York, **1993**.
[47] S. I. Van Dijk, P. G. Wiering, C. P. Groen, A. M. Brouwer, J. W. Verhoeven, W. Schuddeboom, J. M. Warman, *J. Chem. Soc., Faraday Trans.* **1995**, *91*, 2107.

Received December 27, 2000
[O00663]